Physical studies of Au_xSi_{1-x} amorphous alloys

Ph. Mangin, G. Marchal, C. Mourey, and Chr. Janot
Laboratoire de Physique du Solide, Laboratoire associé au Centre National de la Recherche Scientifique No. 155, Université de Nancy-I, Case Officielle 140, 54037 Nancy Cedex, France
(Received 24 July 1979)

Amorphous films of the system Au_xSi_{1-x} have been prepared by vapor deposition over a wide compositional range ($0<x<0.8$). Their physical properties, their stability in the amorphous state, and the crystallization mechanisms have been investigated by electronic microscopy and diffraction, electrical-resistivity and mass-density measurements. The results are compared with those obtained in the liquid alloys, liquid quenched glasses, and getter sputtered films of the same system. Some similarities in short-range orders of all these materials are suggested especially near the eutectic composition. The present study would also suggest that Au-rich alloys near the Au_3Si composition (a-μ phase) have a close-packed metallic structure, while the alloys of the Si-rich end exhibit a more open continuous-random-network-like structure with Au atoms in interstitial sites (a-Si phase), amorphous alloys in the intermediate-composition range being an intricated mixture of both a-μ and a-Si phases. Before reaching the equilibrium dissociation into crystalline Au and Si, crystallization occurs via a diffusionless transformation into a crystalline c-μ phase (alone or with silicon) whose short-range order is compared with that of the a-μ phase. Electrical properties and stability are discussed within the framework of this model.

I. INTRODUCTION

The existence of a deep eutectic in the equilibrium phase diagram has been long suspected as a crucial factor in obtaining an amorphous material by quenching a liquid. Large viscosity at relatively low temperature in the liquid eutectic is indeed favorable to solidification without crystallization.[1]

This rule has been verified for several systems, especially for Au_xSi_{1-x} alloys[2,3] for which the eutectic is so deep that the melting point is 370 °C at $x=0.81$,[4] and reaches 600 °C for differences of about ±0.05 in composition. In addition, this binary system has a very simple phase diagram with miscibility gap in the solid state over the whole range of composition.[5] This is probably the reason why Au_xSi_{1-x} glasses near the eutectic concentration have been prepared and studied for a long time.[2,3] Since then, amorphous Au_xSi_{1-x} alloys have been obtained over a wider concentration range than liquid quenched glasses (g-Au_xSi_{1-x}) either by getter sputtering (s-Au_xSi_{1-x}) (Ref. 6) or vapor deposition (v-Au_xSi_{1-x}).[7,8]

As we have been able to extend the compositional range of stability for this amorphous alloy from pure silicon to $x\simeq 0.80$ and as both investigation techniques and ideas have largely gone through evolutions, one would like to propose some sort of balance sheet regarding the following properties:

Stability as a function of composition, temperature, and preparation method.

Structural description as obtained from diffraction traces and mass-density measurements.

Electrical properties in relation with short-range and long-range structure near the eutectic composition and towards Si-rich composition (metal→nonmetal transition).

Crystallization via a series of both diffusionless and diffusion-controlled transformation.

In this paper data collected in the present work will be critically compared to previous results and a structural model will be proposed as a synthesis.

II. OBTAINMENT CONDITIONS FOR Au_xSi_{1-x} AMORPHOUS ALLOYS

A. Experimental procedures

As the preparation technique may influence the structure of the obtained amorphous material it is of importance to describe briefly the various procedures that have been used, mainly quenching from the liquid,[2,3] vapor quenching after sputtering,[6] or evaporation.[7,8] As described by Hauser *et al.*[6] alloy films were getter sputtered with an argon pressure of about 3×10^{-2} Torr onto sapphire substrates held at 77 K. The sputtering targets were prepared by inductively melting gold and silicon in the proper proportion.

In the work of Hiraki *et al.*[7] and Kishimoto *et al.*[8] evaporations from a single crucible have been carried out by electron beam bombardment in a vacuum which is claimed to be better than 10^{-9} (Ref. 7) or 2×10^{-7} Torr.[8,9] Substrates were tantalum or glass plates whose temperature has not been reported. In both sets of methods the actual composition of the alloys has to be post-determined by the atomic absorption spectro-

photometry or with the help of x-ray fluorescence.

In the present work samples were prepared in an ultrahigh-vacuum chamber by simultaneous condensation on cooled substrates (77 K) of gold and silicon evaporated from separate electron beam crucibles. The pressure was better than 3×10^{-8} Torr during the evaporation process, the ultimate vacuum of the apparatus being 10^{-9} Torr. The evaporation rates of the two components were measured and controlled by two quartz monitoring systems (QMS) whose vibration period is a linear function of the deposited mass. Thus alloy composition can be determined after calibration using aluminum evaporated films (Fig. 1). Substrates were simple glass plates with gold electrodes for resistivity measurements, optically polished glass plates for thickness data, and carbon coated grids for electron microscopy investigations.

B. Compositional range of existence

Results are summarized in Fig. 2 according to the preparation method. Quenching from the liquid[10] gives rise to amorphous Au_xSi_{1-x} alloys if $0.60<x<0.83$. On the Au-richer side quenched materials are crystallized and Si-richer alloys have too high a liquidus temperature.

Getter sputtered amorphous films have been obtained from $x=0.50$ to $x=0.87$ (Ref. 6). In Refs. 7 and 8 Au_xSi_{1-x} obtained by the evaporation technique have been presumed amorphous over the range $0<x<0.30$ without proper physical checking (resistivity transition or diffraction trace). In the present work the evaporation deposited films have been found amorphous in electron diffraction and resistivity over the composition range $0<x<0.8$; $x>0.80$ results in a quenched crystallized alloy.

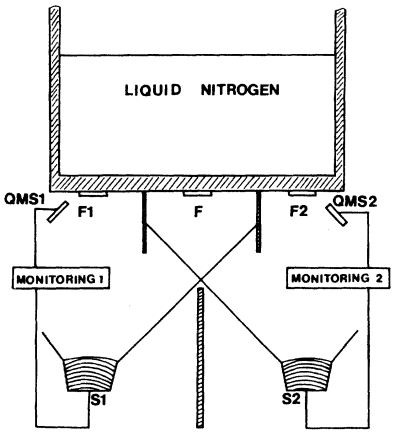

FIG. 1. Evaporation arrangement. QMS1, QMS2: quartz monitoring systems; $S1$: gold source, $S2$: silicon source; F: Au_xSi_{1-x} film; $F1$, $F2$: pure gold and pure silicon films.

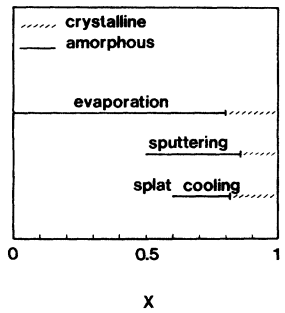

FIG. 2. Sketchy representation of the stability range of the Au_xSi_{1-x} amorphous alloys obtained by various methods.

C. Temperature dependence of stability

The crystallization temperatures of Au_xSi_{1-x} amorphous alloys have been scarcely measured and are shown in Fig. 3. g-Au_xSi_{1-x} (Refs. 2, 3, and 10) is transformed into crystalline material at room temperature within a few hours. s-Au_xSi_{1-x} starts to crystallize above 373 K and transformation is completed within 20 min at 550 K.[6] As described in Sec. IV of this paper, we have measured the crystallization temperature T_c of the v-Au_xSi_{1-x} (see the curve in Fig. 3). Starting from room temperature for $x\simeq0.80$, T_c exhibits a sharp increase over the ranges $0.6<x<0.8$ and $0<x<0.30$ with an obvious smaller slope in the intermediate compositions.

Thus g- and v-Au_xSi_{1-x} near the eutectic composition crystallize at the same temperature (~room temperature). The apparent greater stability of the s films, according to Hauser himself,[6] is undoubtedly caused by the incorporation of argon (~1%) during deposition.

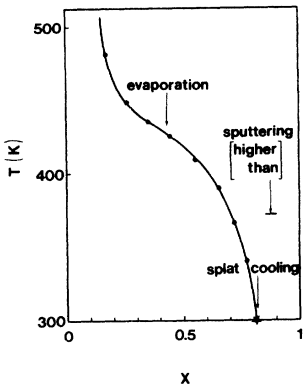

FIG. 3. Compositon dependence of the crystallization temperature.

III. STRUCTURAL APPROACH

Again, structural studies of the Au_xSi_{1-x} amorphous systems have been mainly restricted to summary diffraction traces near the eutectic composition and down to $x \simeq 0.5$. In this section electron diffraction profiles and mass-density measurements will be reported and analyzed in detail.

A. Diffraction traces and interference functions

1. g-Au_xSi_{1-x}

According to Chen and Turnbull[3] the x-ray diffraction patterns show a broad peak characteristic of an amorphous structure at the diffusion vector $k_p = 2.76$ Å^{-1}. Dixmier and Guinier data[10] are in qualitative agreement with the previous authors. It is worth noting that there is no splitting (or shouldering) of the second maximum, contrary to that found in many amorphous metal-metalloid alloys near the eutectic composition.[11] Without going into detail, it is mentioned in Ref. 10 that enrichment with silicon results in a broadening of the first ring.

2. s-Au_xSi_{1-x} (Ref. 6)

Hauser *et al.*[6] have restricted their published data to the recorded intensity around the first ring of their diffraction patterns. This first peak culminates at $k_p = 2.76$ Å^{-1} if $x \simeq 0.87$ is not sensibly shifted down to $x \simeq 0.69$, at which a significant broadening can be observed especially on the short wave vector side, and finally splits into two maxima situated at $k_p = 2.9$ Å^{-1} and $k'_p \simeq 2.25$ Å^{-1} for $x \simeq 0.5$. The authors claim that this broadening and, finally, splitting is caused by the progressive occurrence of more and more covalent tetrahedral bondings among silicon atoms.

3. v-Au_xSi_{1-x} (present work)

The interference functions have been obtained for amorphous alloys (from $x = 0$ to $x = 0.80$), using electron diffraction traces as previously described.[12,13] Compared to x-ray or neutron techniques this method suffers from basic inaccuracy in the absolute intensities, but gives a correct description of shapes and positions of the diffraction rings.

Experimental data are shown in Fig. 4. For the alloys of the gold-rich side the interference functions have a sharp maximum at $k_p = 2.78$ Å^{-1} with a weaker unsplit maximum at $k'_p = 4.9$ Å^{-1}. Enrichment with silicon results first in broadening and then in the progressive appearance of two satellite peaks, situated on each side of k_p, at $k_1 = 2.10$ Å^{-1}, and $k_2 = 3.60$ Å^{-1}. Near pure amorphous silicon, k_p has been completely erased and (k_1, k_2)

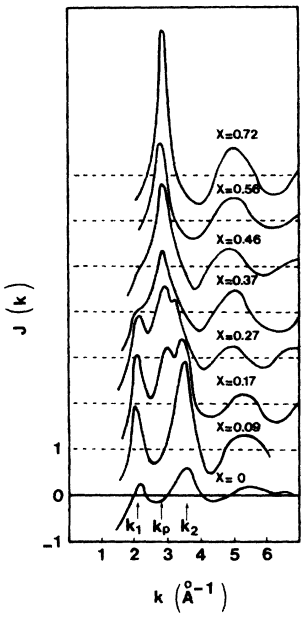

FIG. 4. Interferences functions $J(k)$ obtained with v – Au_xSi_{1-x}.

are the remaining major maxima of the interference functions of pure silicon.[14]

Thus the main features as pointed out in Sec. III A are the following:

(a) Near the eutectic composition the interference function has a broad maximum at $k_p \simeq 2.75$ Å^{-1} whatever the preparation method used and, when reported, the second maximum is unsplit.

(b) Again in the three cases, enrichment by 10–15% silicon has no drastic consequences except for broadening of the peak bottom.

(c) Upon further enrichment with silicon the interference functions as reported in the present work transform themselves into a sort of weighted superposition of two partial patterns that can be respectively ascribed to "amorphous eutectic," referred as a-μ phase in the following, and basically amorphous silicon-like material.

On the other hand Waghorne *et al.*[15] have measured diffraction traces in $Au_{0.815}Si_{0.185}$ liquid alloy and have found a first maximum at $k_p = 2.75$ Å^{-1}, and a second unsplit one at $k'_p \simeq 4.8$ Å^{-1}; this is very similar to that observed in amorphous materials near the eutectic composition. These authors have calculated a radial distribution function and have interpreted their results in a close-packed model with more than ten nearest neighbors.

B. Mass-density measurements

To our knowledge any mass-density measurements have not been reported before in Au_xSi_{1-x}

amorphous alloys. It is well known that such an accurate investigation suffers from drastic experimental difficulties. Density measurements on amorphous films require the determination of both thickness e and mass m of unit area samples.

Thicknesses e were about 2000–2500 Å and directly determined by multiple beam interferometry[16] with an error less than ±15 Å. Careful mass[17] calibration of both QMS (used as balances) were carried out by scaling the QMS indications with the mass of deposited aluminum films which can be calculated from measured thickness values and the Al density considered as being the same for evaporated films and bulk material (data from Ref. 18 modified by conclusions of Ref. 17). To test this calibration procedure, the density of pure gold films has been measured and found to be the same as in bulk material (with difference less than 1%). Moreover, to ascertain the mass of the amorphous Au_xSi_{1-x} alloys with a greater precision and in particular to do away with time shift or statistical fluctuations of the regulation system, pure gold ($F1$) and pure silicon ($F2$) films were simultaneously deposited on two subsidiary substrates; the directly measured thicknesses of these pure films have been used as a permanent control of the QMS indications (see Fig. 1).

In Table I are reported the density data measured at room temperature and the number N of atomic moles per cm^3 which is easily calculated from the density. In Fig. 5 are shown the compositional dependence of N in the amorphous alloys along with the N values in pure crystalline gold, pure crystalline silicon, and pure liquid silicon

TABLE I. Experimental data for density and atomic density of Au_xSi_{1-x} amorphous alloys (a-Au_xSi_{1-x}), crystalline gold (c-Au), crystalline silicon (c-Si), and liquid silicon (l -Si) at the melting point.

	x	density	N(atomic moles cm^{-3})
c-Au		19.3	0.0979
a-Au_xSi_{1-x}	0.80	15.43	0.0947
	0.75	14.98	0.0964
	0.70	13.73	0.0938
	0.635	12.94	0.0954
	0.53	10.76	0.0917
	0.33	7.58	0.0900
	0.19	5.27	0.0870
	0.09	3.75	0.0837
	0.05	2.90	0.0798
	0.00	2.20	0.0785
c-Si		2.32	0.0826
l-Si (Ref. 37)		2.51	0.0893

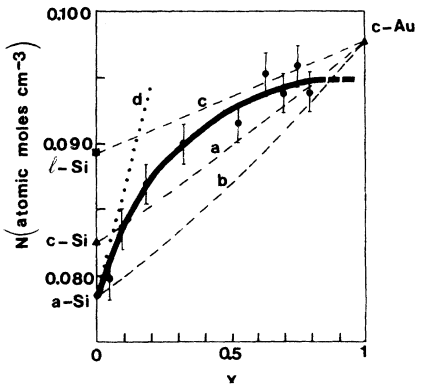

FIG. 5. Compositional dependence of the atomic density: measured in $v-Au_xSi_{1-x}$ alloys (full line and ●). Calculated for a mixture of (a) crystalline gold and silicon (dashed line): for a mixture of c-Au and a-Si [dashed (b) line]; for a mixture of c-Au and liquid Si [dashed (c) line]. Expected from purely interstitial solution of Au in a-Si [dotted (d) line].

at the melting point; hypothetical dashed lines have been drawn to picture the expected composition dependences of N in a mixture of crystalline gold and crystalline silicon (a curve), in a mixture of crystalline gold and amorphous silicon (b curve), and in a mixture of crystalline gold and liquid silicon at its melting point (c curve).

If we look at our data with a "semiconductor point of view," meaning at the Si-rich end of Fig. 5, the most prominent features are the following:

(1) According to N values in pure silicon, the packing fraction is only 5% less in amorphous than in crystalline material which is very close to the calculated value from the continuous-random-network (CRN) model[19] and in good agreement with recent experimental data.[20] The high packing of the material obtained here can certainly be ascribed to the preparation conditions (a slow evaporation rate <10 Å sec^{-1} and a good vacuum).

(2) Alloying gold to silicon in the amorphous state up to $x \simeq 0.1$ results in an increase of the atomic density larger than expected from mixing crystalline gold and amorphous silicon (b curve) and not too far from values calculated for a pure interstitial model (dotted d curve) in which gold atoms would simply fill the holes of the CRN structure. Thus, growth of small noble-metal crystallites in the amorphous silicon matrix during quenching can be denied.[21]

On the metal-rich side, quite a different behavior can be pointed out. The atomic density $N = 0.095$ atomic moles cm^{-3} remains practically the same as the Si content varies from 20–40%.

This N value is about 3% less than in pure crystallized gold as expected from the packing fraction of the relaxed dense random packing of hard spheres (DRPHS) model[22] and very consistent with data in metallic glasses materials.[23] Thus it can be stated that the gold-rich Au_xSi_{1-x} amorphous alloys have a close-packed structure up to a concentration of 40-at.% Si and that, contrariwise to the semiconductor end, the addition of silicon in the amorphous metallic alloy is mostly substitutional. Looking again at Fig. 5, it can be suggested that crystallization of the amorphous metallic phase into gold and silicon would result in a volume expansion of a few percent which is just the estimated volume expansion on solidification of the $Au_{0.815}Si_{0.185}$ liquid alloy.[15] This could support the idea of some resemblance between the amorphous phase and the liquid state. Such an analysis of the density data is well supported by the evolution of the interference functions as described in the preceding section.

IV. ELECTRICAL PROPERTIES

The main ideas in measuring the electrical resistivity have been to give evidences of a metal→nonmetal transition on the silicon-rich side and to test the Ziman model on the other side [resistivity maximum and negative temperature coefficient of the resistivity (TCR) $1/\rho\, d\rho/dT$ near the eutectic composition]. As previous similar studies have been restricted to a more narrow compositional range and have been claimed by their authors to suffer a great experimental uncertainty[6] a detailed investigation will be reported here. Resistivity of the as-quenched samples and resistivity changes during aging were monitored with a four-point probe accurate to 0.01%.

Typical experimental resistivity behaviors are pictured in Fig. 6. Label 0 applied to as-quenched state; one-way irreversible behaviors 0→1, 1→3 correspond to relaxation of the amorphous material towards a more stable, still amorphous, state; two-way reversible sequences 1⇄2, 3⇄4... are linear if $x > 0.3$ [Figs. 6(a) and 6(b)] and then give the TCR for each partially relaxed amorphous state but show thermally activated phenomena on the other compositional side ($x < 0.3$) [Fig. 6(c)].

For a particular temperature T_c there is an abrupt irreversible decrease 3→5 in the resistivity which corresponds to crystallization (see Fig. 3) into a metastable phase whose TCR can be measured on 5⇄6. Upon further warming up to T_7, a second transformation results in an additional resistivity irreversible change 5→7 [Figs. 6(a)–6(c)]. For alloy with $x > 0.5$ [Fig. 6(a)] this resistivity recovery is a decrease and a positive TCR in the state labeled 7 can be measured along 7⇄8. On the other side ($x < 0.5$) [Figs. 6(b) and 6(c)] this second resistivity change is an increase and the result is typical of ther-

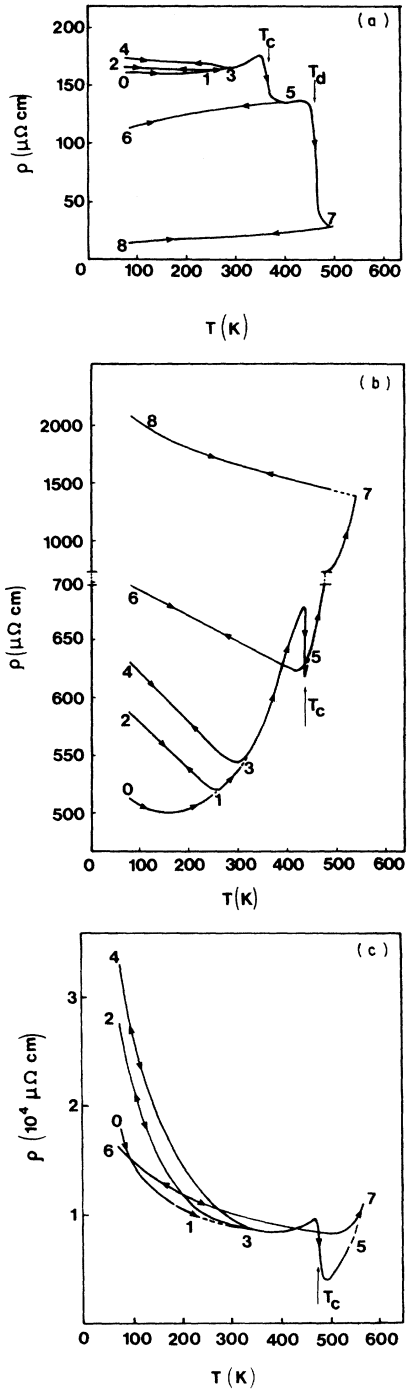

FIG. 6. Typical resistivity behavior in v-Au_xSi_{1-x}: (a) $x = 0.715$, (b) $x = 0.36$, (c) $x = 0.174$.

TABLE II. Resistivity behavior with respect to composition.

T \ x	0	0.1	0.3	0.5	0.8	1
			Structural relaxation in the amorphous phase			
	Thermally activated processes in stabilized amorphous states		$(1/\rho)\,d\rho/dT < 0$ and constant vs T in stabilized amorphous states.			
T_c	Crystallization is not observed in resistivity		Evidence of crystallization via an abrupt irreversible decrease in resistivity			
T_d			Second transition with increase in resistivity and stabilization into a state exhibiting thermally activated processes	Second transition with decrease in resistivity and stabilization into a state with linear $\rho(T)$ and TCR greater than 0		

mally activated processes.

All these experimental data are summarized in Table II and pictured in Fig. 7 which gives the as-quenched resistivity versus composition $\rho_0(x)$, along with s-Au_xSi_{1-x} data[6] and resistivity in liquid,[24] in Fig. 8 which gives the TCR for the amorphous state stabilized at 300 K (which in fact is still valid whatever the annealing temperature), and in Fig. 9 which duplicates Fig. 7 in the logarithm coordinate to allow drawing over the whole composition range and compares the present data with those of Kishimoto *et al.*[8] The activation energies calculated in the range $x < 0.3$ are shown in Fig. 10 along with those given in Ref. 8. In Table III are reported the calculated activation energies at 77 and 300 K for alloys annealed up to 300 K. A reasonable agreement between literature data and the present work can be observed if consideration is given to the difference in preparation method.[25,26]

V. CRYSTALLIZATION OF THE Au_xSi_{1-x} AMORPHOUS ALLOYS

Crystallization of our v-Au_xSi_{1-x} compared to that of g-Au_xSi_{1-x} near the eutectic composition has been the subject of a detailed paper.[27] The main results are summarized in Table IV and the composition dependence of the crystallization temperature T_c as obtained in resistivity measurements is given in Fig. 3. The first transformation at T_c results into a metastable phase, referred to as c-μ phase, which can appear alone around the composition Au_3Si or in a mixture with silicon. This c-μ phase would have an orthorhom-

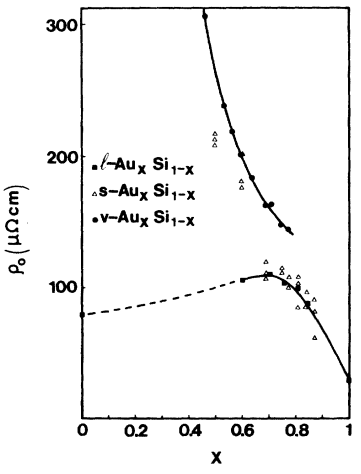

FIG. 7. Composition dependence of the as-quenched resistivity in Au_xSi_{1-x} alloys: ● present work, △ Ref. 6, ■ in the liquid system.

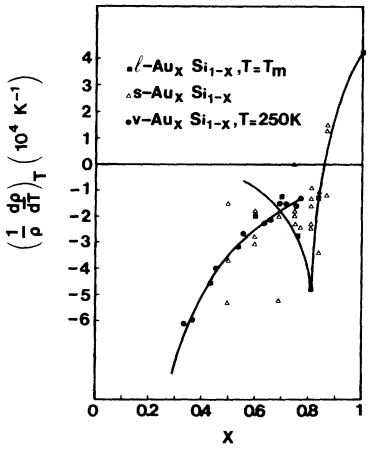

FIG. 8. Temperature coefficient of the resistivity according to Fig. 7.

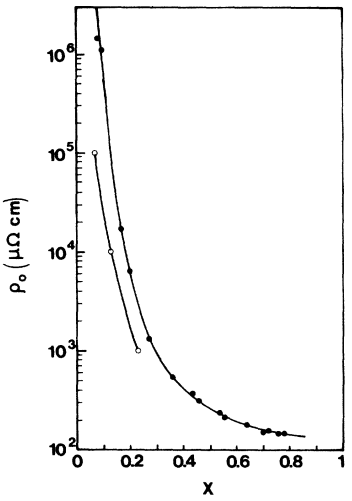

FIG. 9. $\ln\rho(x)$ over the whole range of composition: ● present work, ○ Ref. 8.

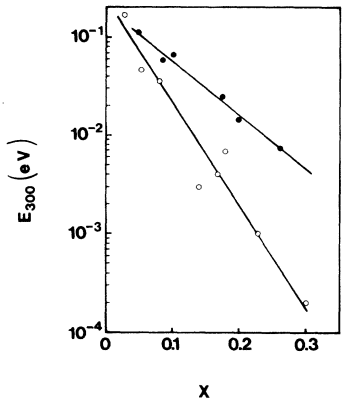

FIG. 10. Composition dependence of the activation energy in resistivity regime below $x<0.3$: ● present work, ○ Ref. 8.

bic structure with $a=12.9$, $b=7.45$, and $c=11.6$ Å, similar to the δ phase of Andersen *et al.*,[28] and which can be described in terms of distorted gold-like sub-cell structures. The so-called c-μ phase, a-μ phase (see Sec. II A), and the eutectic liquid have a similar silver-like color whatever the preparation method, and have comparable mass densities larger than the one of a gold-silicon mixture in the same proportion.[3,28] A second transformation at higher temperature corresponds to the dissociation into crystalline gold and silicon as foreseen by the equilibrium phase diagram.

VI. INTERPRETATION AND DISCUSSION

A. Description of the proposed model

In this section one would like to describe structure, electrical properties, and crystallization of the Au_xSi_{1-x} amorphous alloys in the framework of a model based on the assumption that the a-μ and c-μ phases as well as the liquid near the eutectic composition are characterized by the same short-range order (SRO). This SRO would correspond to favorable stability conditions and consequently the three phases would have a local minimum of their free energy for this composition.

In the liquid phase, adding gold or silicon to the μ eutectic liquid would not change the SRO, since pure liquid silicon has still a close-packed metallic structure, but results in a drastic increase of the free energy, which is consistent with the existence of a deep eutectic in the phase diagram. Contrariwise, silicon would have a strong tendency to become tetrahedrally coordinated for high silicon concentration in amorphous alloys and free energy can be gained by "dissociation" into a-μ and amorphous silicon-like (a-Si) phases, the latter including gold atoms in interstitial positions. The existence of these two amorphous phases must be rather regarded as local fluctuation in structure and composition without true phase interfaces. Such a dissociation into two precursor amorphous phases (a-μ and a-Si) could be explained by the fast diffusion of gold in both amorphous and crystalline silicon even at relatively low temperature.[29,30] Thus the free-energy diagram of the system would be that pictured in Fig. 11. Absolute minima in the free energy correspond of course to crystalline materials c-Si and c-Au. We would like to use this model to interpret the experimental results as given in the preceding sections.

B. Interpretation of the crystallization mechanism

According to the free-energy diagram of Fig. 11, the a-μ and a-Si phases are supposed to crystallize separately into metastable c-μ and c-Si phases without long-range diffusion. Thus the crystallization occurs in place and the c-μ+c-Si material interfaces are as poorly defined as in the amorphous alloy. However, this first transformation results in a decrease in resistivity because of ordering inside the μ phase.

The second transformation, which is the dissociation into gold and silicon, must be controlled by long-range diffusion and results in more separated phases. On the gold-rich side ($x>0.5$), silicon islands are disseminated in a gold sea and the second transformation naturally involves a decrease in resistivity. On the other side ($x<0.5$), the second transformation makes gold clusters in a silicon matrix whose electrical con-

TABLE III. Measured values of the activation energy in v-Au_xSi_{1-x} alloys.

Composition at. % Au	0	0.05	0.086	0.10	0.174	0.20	0.265
E at 300 K (eV)	0.12	0.11	0.06	6.7×10^{-2}	2.5×10^{-2}	1.5×10^{-2}	7.4×10^{-3}
E at 77 K (eV)		0.035	0.016	1.9×10^{-2}	4.9×10^{-3}	3.6×10^{-3}	8×10^{-4}

duction is ruled by thermally activated phenomena with large resistivity (see Table II). The measured atomic composition border $x \simeq 0.5$ between the two regimes corresponds to 45% gold and 55% silicon of the total volume. This result is very similar to that measured in the aluminum-germanium system.[31]

C. Structural description (interference functions and mass density data)

Assuming the diagram of Fig. 11 to be true would result in amorphous material made of mainly the a-μ phase on one side, the a-Si phase on the other side, and a mixture of both phases in the intermediate composition range. Indeed this is well supported by data obtained from diffraction traces and density measurements.

On the gold-rich side the interference functions are very similar between them and with that of the liquid eutectic; mass-density data show that atomic density is fairly constant over the composition range $0.6 < x < 0.8$. This should be the existence range of the a-μ phase, whose structure looks very close packed. Contrariwise to data obtained with Fe_xSi_{1-x} amorphous alloys,[12,32] enrichment of the a-Au_xSi_{1-x} films does not result in a continuous homogeneous transformation of the interference function but involves the appearance of an amorphous Si-like phase. This second phase progressively replaces the a-μ phase and seems to be alone when $x < 0.1$. The atomic density increases with gold content which could be due to gold atoms in interstitial position of a CRN structure. Thus the assumption of gold crystallites into a silicon matrix can be deceiving.[26]

D. Electronic transport properties

In the Ziman model[33] the resistivity of amorphous material reaches a maximum when the diameter $2k_F$ of the Fermi surface is equal to the diffusion vector k_p of the interference function first peak. The TCR is negative when $2k_F \simeq k_p$, and becomes positive for $2k_F$ sensitively larger or smaller than k_p.[34] This model has been qualitatively verified in a recent study devoted to Fe_xSn_{1-x} amorphous alloy,[35] and seems to be relevant for Au_xSi_{1-x} liquid alloys down to $x \simeq 0.5$,[24] addition of silicon involving only a shift of the Fermi level. Looking at the free-energy diagram (Fig. 11) on the gold side shows that the a-μ phase is as homogeneous as the liquid and the Ziman model should be valid. Contrariwise, on the silicon side of the a-μ phase liquid is still homogeneous while the amorphous material is not anymore and applying a Ziman model

TABLE IV. Crystallization processes of the Au_xSi_{1-x} amorphous alloys.

annealing temperature \ x	0	0.2	0.7	0.8	1
below T_c (RT)	Amorphous material				Quenched alloys are already crystallized
just above T_c	Crystalline silicon c-Si+ a-μ phase (?)	c-Si+ c-μ (small crystals)	c-μ phase (large crystals)		
after 2nd transformation in resistivity	Crystalline gold + crystalline silicon				

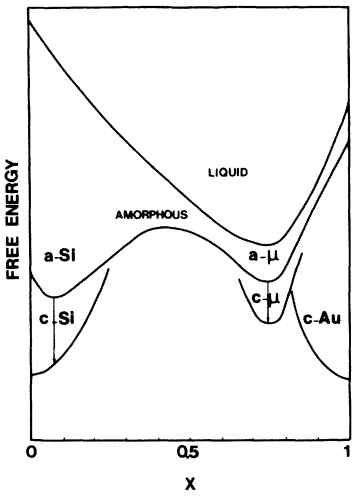

FIG. 11. Hypothetical free-energy diagram for the Au_xSi_{1-x} systems.

would not be sensitive. Indeed the resistivity trend is to increase (Fig. 7) with a negative decreasing TCR (Fig. 8) in the composition range $x \gtrsim 0.70$.

Calculated values of $2k_F$ in the assumption that gold contributes one and silicon four electrons to the conduction band and using density data (Table I) are reported in Table V. $2k_F \simeq k_p = 2.75$ Å^{-1} is reached near the eutectic composition. On the other hand, the resistivity does not decrease on the silicon-rich side and the TCR fails to reach a minimum. Over the composition range $0.3 < x < 0.7$, the electrical conductivity is due to the percolating a-μ phase whose effective cross section decreases upon silicon enrichment. Thus the overall resistivity increases but has mainly the negative TCR of the μ phase. Below $x \simeq 0.3$, the a-μ phase does not percolate anymore and conductivity should be mainly ruled by the a-Si phase. Thus the resistivity increases drastically with an obviously different regime behavior since the mean TCR is -16×10^{-4} for $x \simeq 0.25$ compared to TCR $\simeq -6\times10^{-4}$ for $x \simeq 0.34$. Such an interpretation was one of the suggested ideas of Hauser *et al.*[6] who had presumed the appearance of tetrahedrally coordinated silicon atoms without proposing dissociation into two amorphous phases.

TABLE V. Calculated $2k_F$ values versus composition.

x	1	0.80	0.75	0.70	0.635
$2k_F$ (Å^{-1})	2.40	2.78	2.88	2.935	3.05

According to Kishimoto *et al.*,[25,26] the composition range $x < 0.30$ should be subdivided into two conductivity regimes on each side of $x = 0.14$: (i) hopping regime at low gold concentration, and (ii) appearance of a gold narrow band in the silicon gap for $x > 0.14$.

E. Thermal stability of the amorphous alloys

As shown in Fig. 3 Au_xSi_{1-x} alloys are more and more stable in the amorphous state upon addition of silicon. The T_c (x) curve has a particularly large slope when $x > 0.7$ and $x < 0.3$. The improved stability between $x \simeq 0.8$ and 0.7 might be interpreted in terms of the nearly free electron model of Nagel and Tauc[36] which foretells the best stability when $2k_F \simeq k_p$. On the other side ($x < 0.3$), the increasing prominence of covalent bondings in a percolating a-Si phase is indeed in favor of a great stability. In the intermediate concentration range ($0.3 < x < 0.7$), changes in the total stability may be a compromise between constant stability of the percolation a-μ phase and the appearance of more stable a-Si islands. However, it is not clear why the μ-phase small islands fail to crystallize along with silicon above T_c; it might result from a size effect or kinetic problems. Note an apparent slight discrepancy between density data, which show the a-μ phase between $x = 0.6$ and $x = 0.8$, and resistivity measurements which limit the composition range down to $x \simeq 0.7$. In fact, electrical resistivity is well known as being very sensitive to the least transformation and may probe changes in the a-μ phase structure before the mass density does.

[1]D. Turnbull, J. Phys. (Paris) C4, 1 (1974).
[2]W. Klement, Jr., H. Willens, and P. Duwez, Nature 187, 869 (1960).
[3]H. S. Chen and D. Turnbull, J. Appl. Phys. 38, 3646 (1967).
[4]E. G. Heath, J. Electron. Control 11, 13 (1961).
[5]M. Hansen, *Constitution of Binary Alloys* (McGraw-Hill, New York, 1958), 2nd ed., p. 232.
[6]J. J. Hauser and J. Tauc, Phys. Rev. B 17, 3371 (1978).
[7]A. Hiraki, M. Iwami, A. Shimizu, and K. Shuto, Mater. Sci. Eng. 23, 289 (1976).
[8]N. Kishimoto, K. Morigaki, A. Shimizu, and A. Hiraki, Solid State Commun. 20, 31 (1976).
[9]N. Kishimoto, K. Morigaki, T. Sano, M. Iwami, and A. Hiraki, *Amorphous and Liquid Semiconductors*, edited by W. E. Spear (University of Edinburgh Press, Edinburgh, 1977), p. 490.
[10]J. Dixmier and A. Guinier, Mém. Sci. Rev. Métall. LXIV, 53 (1967).
[11]G. S. Cargill, Solid State Phys. 30, 227 (1975).

[12]Ph. Mangin, G. Marchal, B. Rodmacq, and Chr. Janot, Philos. Mag. 36, 643 (1977).
[13]S. Fujime, Jpn. J. Appl. Phys. 5, 1029 (1966).
[14]S. C. Moss and J. F. Graczyk, Phys. Rev. Lett. 23, 1167 (1969).
[15]R. M. Waghorne, V. G. Riylin, and G. I. Williams, J. Phys. F 6, 147 (1976).
[16]S. Tolansky, *Multiple-Beam Interferometry of Surfaces and Films* (Oxford University Press, London, 1948), p. 135.
[17]K. H. Behrndt, J. Vac. Sci. Technol. 8, 622 (1971).
[18]T. E. Hartman, J. Vac. Sci. Technol. 2, 239 (1965).
[19]D. E. Polk, J. Non-Cryst. Solids 5, 365 (1971).
[20]R. Mosseri, C. Sella and J. Dixmier, Phys. Status Solidi A 52, 475 (1979).
[21]E. Haug, N. Hedgecock and W. Buckel, Z. Phys. B22, 237 (1975).
[22]D. S. Boudreaux, Phys. Rev. B 18, 4039 (1978).
[23]Y. Waseda, *Rapidly Quenched Metals III*, edited by B. Cantor (Metals Society, 1978), p. 352.
[24]E. Hauser, S. Ray, and J. Tauc, Solid State Commun. 29, 821 (1979).
[25]N. Kishimoto and K. Morigaki, J. Phys. Soc. Jpn. 46, 846 (1979).
[26]N. Kishimoto and K. Morigaki, J. Phys. Soc. Jpn. 46, 497 (1979).
[27]G. Marchal, Ph. Mangin and Chr. Janot (unpublished).
[28]G. A. Andersen, J. L. Bestel, A. A. Johnson, and B. Post, Mater. Sci. Eng. 7, 83 (1971).
[29]B. Tuck, *Introduction to Diffusion in Semiconductors* (Perigrinus, New York, 1974), Ltd. Ed., p. 225.
[30]U. Koster, D. R. Campbell, and K. N. Tu, IBM Research Report No. RC 7085, 1978 (unpublished).
[31]G Deutscher, M. Rappaport, and Z. Ovadyahu, Solid State Commun. 28, 593 (1978).
[32]Ph. Mangin and G. Marchal, J. Appl. Phys. 49, 1709 (1978).
[33]J. M. Ziman, Philos. Mag. 6, 1013 (1961).
[34]H. J. Guntherodt, Adv. Solid State Phys. 17, 25 (1977).
[35]Ph. Mangin and G. Marchal, Phys. Lett. 68A, 466 (1978).
[36]S. R. Nagel and J. Tauc, Phys. Rev. Lett. 35, 380 (1975).
[37]C. Smithells, *Metals Reference Handbook* (Butterworths, London, 1976), 5th ed., p. 945.